Second International Conference on Geotechnique, Construction Materials and Environment,
Kuala Lumpur, Malaysia, Nov. 14-16, 2012, ISBN: 978-4-9905958-1-4 C3051

Effects of Slope Inclination on the Rain-induced Instability of Embankment Slopes

Chaminda Gallage[1], Shiran Jayakody[1] and Taro Uchimura[2]

[1]Queensland University of Technology, Brisbane, Australia
[2]The University of Tokyo, Tokyo, Japan .

ABSTRACT

Rainfall has been identified as one of the main causes for embankment failures in areas where high annual rainfall is experienced. The inclination of the embankment slope is important for its stability during rainfall. In this study, instrumented model embankments were subjected to artificial rainfalls to investigate the effects of the slope inclination on their stability. The results of the study suggested that when the slope inclination is greater than the friction angle of the soil, the failure is initiated by the loss of soil suction and when it is smaller than the friction angle of the soil, the failure is initiated by the positive pore water pressure developed at the toe of the slope. Further, slopes become more susceptible to sudden collapse during rainfall as the slope angle increases.
.

Keywords: Embankment model tests, instrumentation, soil suction, transient seepage, rain-induced slope failures

1. INTRODUCTION

Embankments are very useful geo-engineering structures that are widely used to support roads and rails. They are constructed by shaping the natural slope or by compacting the imported soils. Failure of these embankment slopes can cause for human casualties as well as negative impacts on a country's economy. Most embankment slopes are initially unsaturated prior to any rainfall. In addition to triggering by earthquakes, rainfall has caused the failure of many embankment slopes, worldwide [1]-[4].

Reference [5] performed a series of parametric studies to understand the significance of hydrological and geotechnical parameters of a slope on its rain-induced instability. The study revealed that rainfall, rainfall intensity, soil properties, location of the ground water table, and the slope geometry (angle, height) play a significant role in the rain-induced instability of a slope. Angle and height of an embankment are two key geometrical parameters that control the extent of the area covered by the embankment slope and its stability. In developed/developing area areas, there is a great demand to reduce the area covered by the embankment slopes and hence the embankments are constructed with steeper slopes and in some occasions geo-reinforced embankments are constructed with vertical slopes [6].

Unsaturated embankment slopes can be stable with very steep slope angle until it is exposed to rainfall. The mechanism of slope failure induced by rainfall can vary depending on the slope angle. It is important to understand the mechanism and initiation of failure of an embankment slope to provide better countermeasures against the failure. This paper presents the results of the embankment model tests conducted to investigate the effects of slope angle on the mechanism and the initiation of the failure the of embankment slope subjected to rainfall. Two instrumented model embankment slopes with two different slope angles (e.g. 30^0 and 60^0) were subjected to artificial rainfall until the failure.

2. TESTING MATERIALS

Edosaki soil procured from a natural slope in Ibaraki prefecture in Japan was employed in the experimental work of this study. Wet sieving and hydrometer analyses were performed on this material as it contains fines (particles finer than 0.075 mm) content of 17.1 %. The grain-size distribution curve of the test material is shown in Figure 1. The specific gravity, maximum void ratio, and minimum void ratio of the soil were measured as 2.75, 1.59, and 1.01, respectively. The soil was found to be non-plastic. The optimum gravimetric water content and the maximum dry density of the sand obtained from the standard proctor compaction test were 16.5% and 1.725 g/cm^3 respectively. According to the Unified Soil Classification System, the soil can be classified as silty sand

2.1 Soil Water Characteristic Curves (SWCCs)

Figure 2 depicts the soil-water characteristic curve (SWCC) for Edosaki sand obtained in the laboratory using a Tempe pressure cell. Both the drying and the wetting SWCCs were obtained for the test material using a sample with dry density of 1.22 g/cm^3. Model slopes were constructed using Edosaki sand to achieve dry density of 1.22 g/cm^3.Since the air-entry value of the ceramic disk used in Tempe pressure cell is 300 kPa, the measured SWCCs were restricted to the maximum suction of 200 kPa. More details about SWCC measurement using Tempe pressure cell is given in [7]. As shown Figure 2, the laboratory measured SWCC data were fitted using the equation proposed by Fredlund and Xing [8].

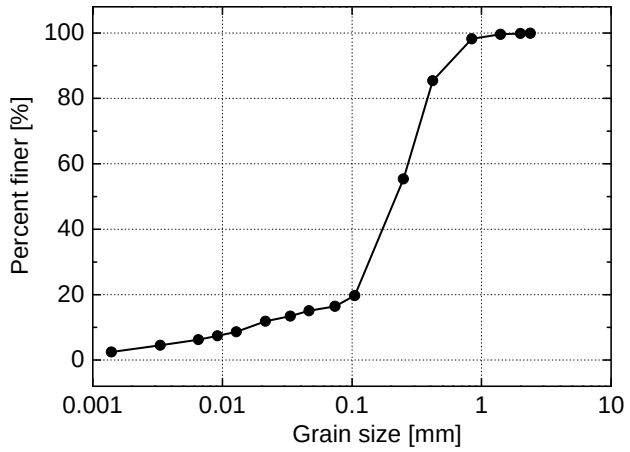

Figure 1. Grain size distribution curve of Edosaki soil

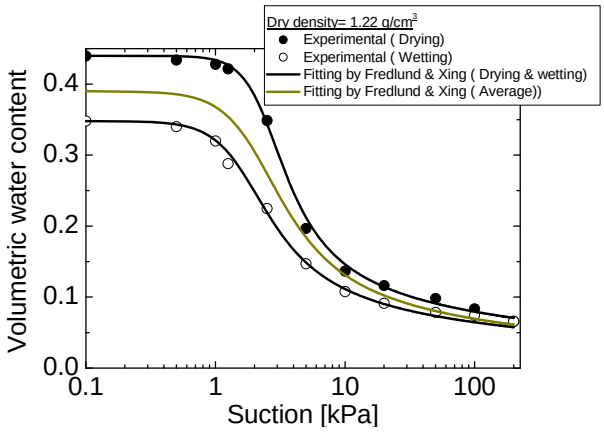

Figure 2. SWCCs of test material

2.2 Unsaturated Permeability

Permeability function of unsaturated soils was measured using a laboratory developed permeameter based on steady –state method [9]. Figure 3 shows the variation of measured coefficient of permeability with suction following the drying path of the SWCC. The test was conducted on the dry density of 1.22 g/cm^3 of Edosaki sand. Figure 3 also compares the laboratory measured permeability function with the predictions using the methods proposed by Fredlund [10], Green & Corey [11], and Van Genuchten [12] (all three methods are included in SEEP/W -2004).

2.3 Unsaturated Shear Strength

A conventional direct shear apparatus was modified to measure unsaturated shear strength under controlled suction. Figure 4 (a) depicts the variation of the ϕ' with the suction. The ϕ' was obtained from both saturated and unsaturated consolidated drained tests employing the modified direct shear device. The results suggested that the effects of suction on the ϕ' is not significant. However, as shown in Figure 4 (b), the apparent cohesion (c) increases with the suction in a decreasing rate.

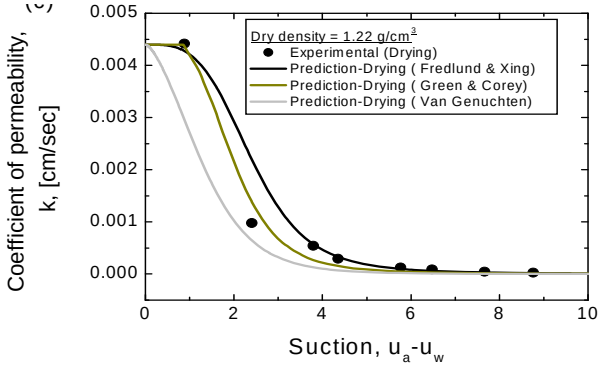

Figure 3. Measured and predicted permeability function of test material

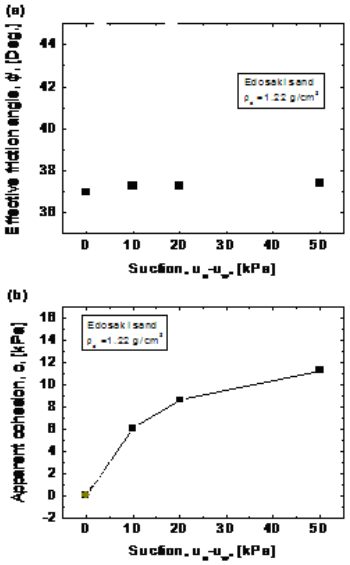

Figure 4. Measured unsaturated shear strength properties of test material

3. MODEL TESTS

In order to examine the effects of slope inclination on the mechanism of rain-induced slope (embankment) failures, two instrumented model tests with two different slope inclinations (i.e. 30^0 and 60^0) were subjected to an artificial rainfall until the failure of the slope. Pore-water pressures, volumetric water contents, soil displacements were monitored continuously at different locations on and in the slope during the construction of the slope and the application of the rainfall.

3.1 Instruments Used

The tank (Figure 5) used in model test has a length of 2.0 m, width of 0.8 m, and a height of 1.0 m. The walls of the tank are made up of steel plates, except for the front side which is made of acrylic glass for easy observation of deformation processes.

ADR (Amplitude Domain Reflectometry) and ECHO types soil moisture sensors were used in the model tests to measure

soil moisture content during water infiltration. In order to measure both positive and negative water pressures, KYOWA 05 PMG pressure sensors were modified with a ceramic cup of 100 kPa air-entry value. Figure 6 shows the types of sensors used in the model tests. LVDTs were used to measure the local displacements on the slope surface. Inclinometers installed in the soil measured the sub-soil displacements. Evaflow side spray irrigation tube (hole size, 0.1 mm) was used to simulate rainfall as shown in Figure 5.

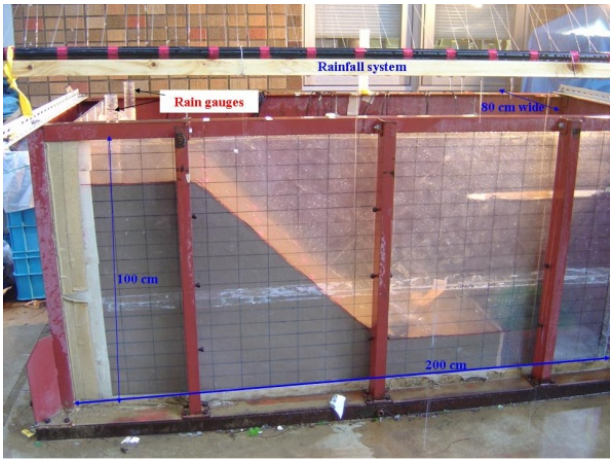

Figure 5. Tank used for model tests

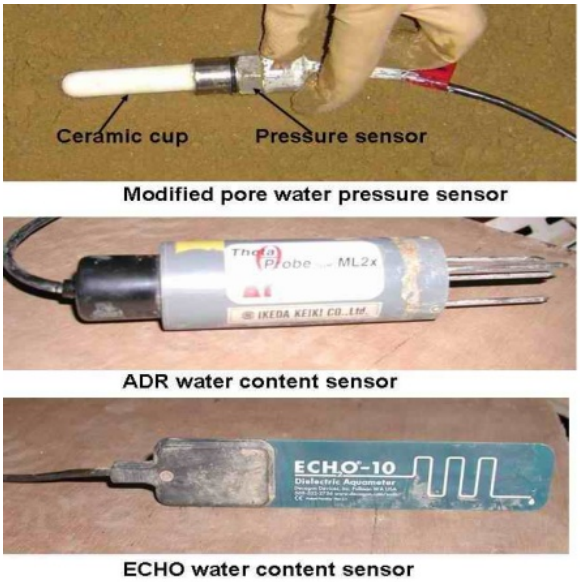

Figure 6. Sensors used in model tests

3.2 Model Preparation

Two model embankments with different slope inclinations (e.g. 30^0, 60^0) were constructed by compacting Edosaki sand with the initial gravimetric water content of 13.5 %. The compaction was performed in order to achieve the dry density of 1.22 g/cm^3. 15 pore-water pressure sensors, 15 water content sensors, three inclinometers, and two LVDTs were installed in each model embankment. All the sensors were connected to a data acquisition system for continuous logging of data during the construction of the slope and as well as during rainfall application.

3.3 Rainfall Simulation

Approximately 24 hours after the completion of the construction of the slope, the slope was subjected to a rainfall with an approximate intensity of 40 mm/hr. During the rainfall application, it was set to log data for every 2 seconds from all the sensors connected with the logging system. Evaflow side spray irrigation tube system used in this experiment was able to provide a relatively uniform constant rainfall between 20 mm/hr and 50 mm/hr. It was able to control the rainfall intensity by regulating the pressure of the water supplied to the system. This rainfall system was calibrated to give different rainfall intensities with supplied water pressure. Four measuring cylinders (rain gauges) were used to measure intensity of rainfall; two of them were positioned near the toe and the other two were placed on the top of the embankment. The rainfall intensity mentioned in this study was calculated by averaging the measured rainfall over the entire duration of rainfall and the numbers of measuring points. To minimize the possible fluctuation of rainfall intensity with time and space (due to wind), the rainfall was applied in the morning (e.g., 5.30 a.m) in most tests.

4. RESULTS AND DISCUSSIONS

Figure 07 shows the locations of the different transducers (pore-water pressure, water content, and horizontal displacement) installed in the model slope which has an inclination of 30^o. At the beginning of the artificial rainfall of 40 mm/hr, the slope was in unsaturated conditions with the suction of 6 ~ 12 kPa (Figure 8(a)) and corresponding volumetric water content 0.2 ~ 0.15 (Figure 8(c)). As the rainfall progressed, the water contents and the pore-water pressures at the different locations in the slope increased as shown in Figure 8(b) and (a), respectively. The lower part of the slope became saturated first forming a water table below the toe area of the slope. As shown in Figure 8(c), the horizontal deformation of the slope started when the toe of the slope was saturated (P8 registered positive value by the time the deformation started) at about 5000 sec after the beginning of rainfall. The deformation seemed to be progressive (Figure 9) with the rise of water table. The rate of horizontal slope displacement was measured to be 3.4 ~ 7.9 mm/hr.

A slope with an inclination of 60^o was constructed and instrumented as shown in Figure 10. Once the slope was subjected to an artificial rainfall of 45 mm/hr, as shown in Figure 11(c), the horizontal deformation of the slope (D1, D2, and surface at inclination 3 (Incli.3)) began with a rate of about 14.4 mm/hr even before the water table rose up to the level of P10 and P8 (Figures 11(a) & (b)). Cracks appeared at the top (crest) of the slope with the start of deformation (at about 2000 sec after the beginning of rainfall). Within 1000 sec after the cracks appearance at the top, the entire slope collapsed as shown in Figure 12. It was interesting to observe that the most part of the slope was unsaturated (the water front

did not reach some areas) by the time the entire slope collapse. It seemed that this failure was initiated by the decrease in the shear strength of the slope due to the loss of soil suction. An unsaturated slope with the inclination greater than the friction angle of the soil can be stable until the suction is decreased by the rain water infiltration into the slope.

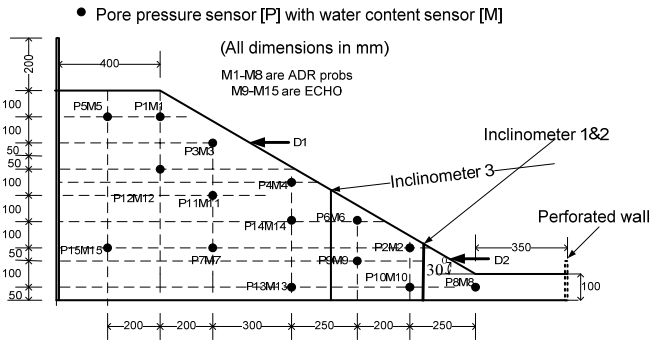

Figure 7. Sensor locations in model test with 30^0 inclination

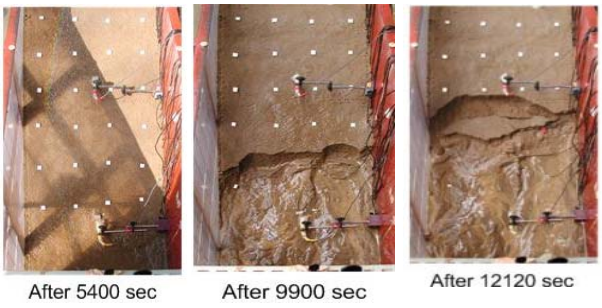

Figure 9. The progress of the failure of the slope with 30^0 inclination

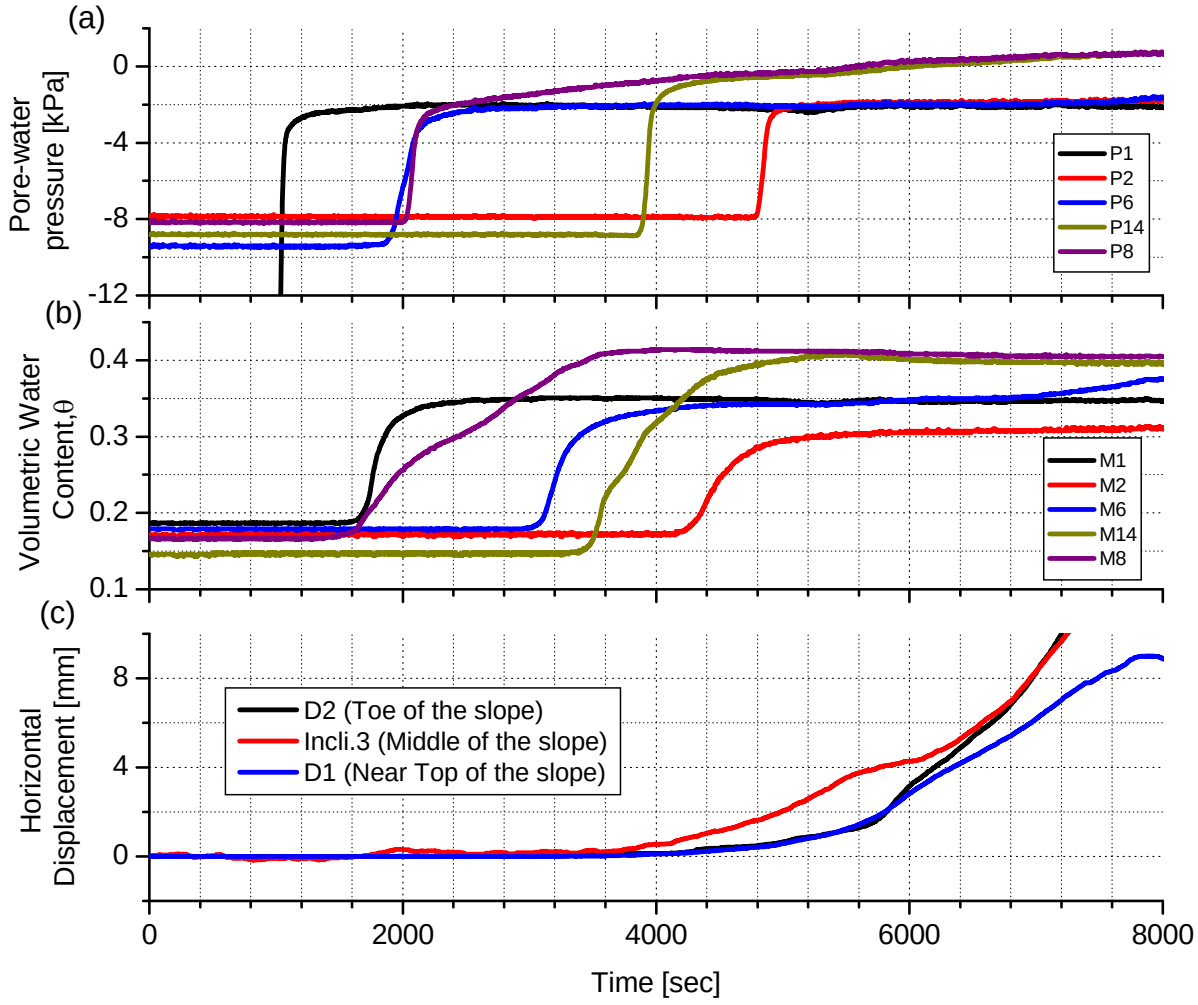

Figure 8. Time histories of: (a) pore-water pressure; (b) volumetric water content; and (c) displacement at various locations of the slope with 30^0inclination

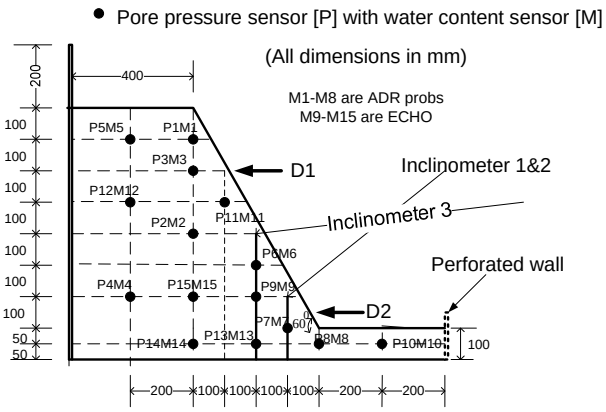

Figure 10. Sensor locations in model slope with 60^0 Inclination

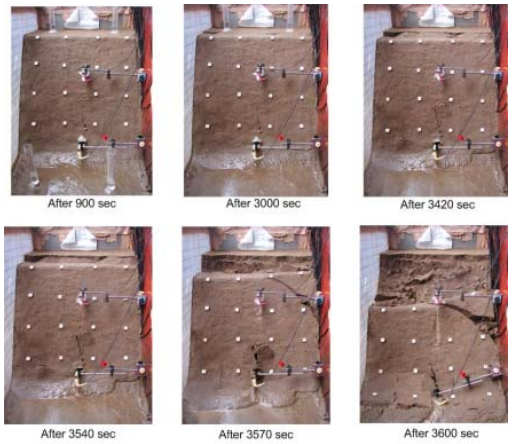

Figure 12. The progress of the failure of the slope with 60^0 inclination

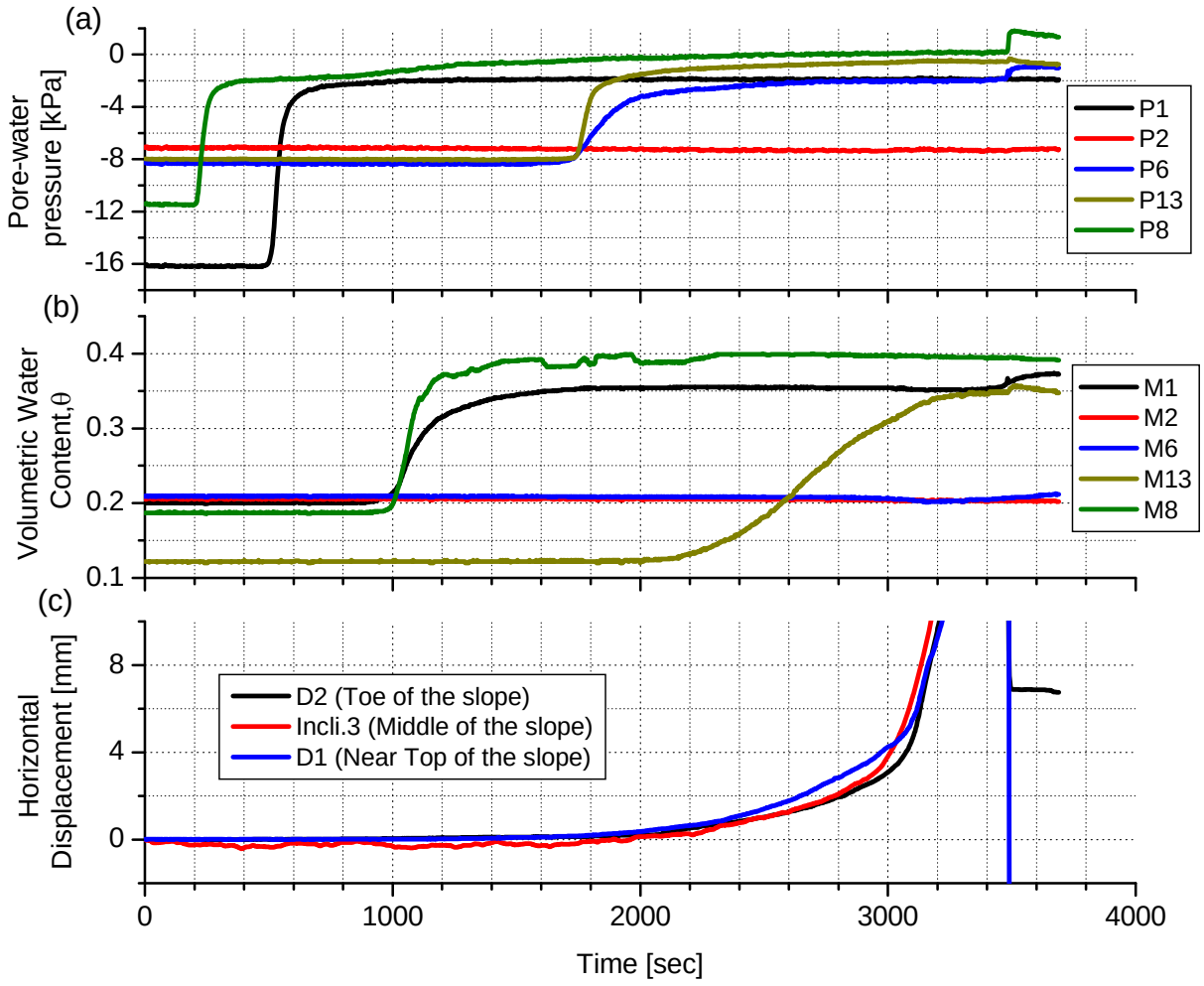

Figure 11. Time histories of: (a) pore-water pressure; (b) volumetric water content; and (c) displacement at various locations of the slope with 60^0inclination

5. CONCLUSIONS

The following conclusions can be drawn from this experimental investigation:

- Slopes become more vulnerable to sudden collapse with the increase in their inclinations.
- Failures of gently slopes are initiated by the development of positive pore-water pressure near the toe and the failure is relatively slow and progressive.
- In the case of steep slopes (especially when slope inclination is greater than the soil's friction angle), the decrease in suction is a predominant factor for the failure initiation.

REFERENCES

[1] Kunio, K. and Hiroakai, S. (1989). "Embankment design in mountainous area with heavy rainfall." Soils and Foundations, 29(4), 35 – 48.

[2] Okada, K. and Sugiyama, T. (1994). "A risk estimation method of railway embankment collapse due to heavy rainfall." Structural Safety, 14(2), 131-150

[3] Aleotti, P. (2004). " A warning system for rainfall-induced shallow failures." Engineering Geology, 73(4), 247 – 257.

[4] Ng, C.W.W. and Zhan, L.T. (2007). "Comparative study of rainfall infiltration into a bare and a grassed unsaturated expansive soil slope." Soils and Foundations, 47(2), 207–217.

[5] Rahardjo, H., Ong, T. H., Rezaur, R. B., and Leong, E. C. (2007). "Factors controlling instability of homogeneous soil slopes under rainfall." Journal of Geotechnical and Geoenvironmental Engineering, 133 (12), 1532–1543.

[6] Tatsuoka, F. (2011). "Developments of geosynthetic-reinforced soil technology in Japan: Retaining walls and bridge abutments". Proceeding of First International Conference on Geotechnique, Construction Materials, and Environment, Mie, Japan.

[7] Gallage, C. P. K., and Uchimura, T. (2010). "Effect of dry density and grain size distribution of soil-water characteristic curve of sandy soils." Soils and Foundations, 50(1), 161-172.

[8] Fredlund, D. G., and Xing, A. (1994). "Equation for the soil-water characteristic curve." Canadian Geotechnical Journal, 31, 521-532.

[9] Klute, A. (1965). "Laboratory measurement of hydraulic conductivity of Unsaturated soil." *In methods of soil analysis*, Mono. 9, Part 1, Amer. Soc. Of Agronomy, Madison, WI, 253-261.

[10] Fredlund, D. G., Xing, A., and Huang, S. 1994. Prediction of the permeability function for unsaturated soils using the soil-water characteristic curve, Canadian Geotechnical Journal, 31: 533-546.

[11] Green, R. E., and Corey, J. C. (1971). "Calculation of hydraulic conductivity: A further evaluation of some predictive methods." Soil Science Society of America Proceedings, 35, 3-8.

[12] Van Genuchten, M. T. (1980). "A closed-form equation for predicting the hydraulic conductivity of unsaturated soils." Soil Science Society of American Journal, 44: 892-898.